ARTICLES

Plasma–wall interaction in an oblique magnetic field: Model of the space-charge sheath for large potentials and small Debye lengths

E. Ahedo
E.T.S.I. Aeronáuticos, Universidad Politécnica, Madrid, Spain

(Received 4 May 1999; accepted 6 August 1999)

An analytical model of the space-charge sheath around a planar wall is derived for the case of (i) uniform magnetic field **B** incident at any angle into the wall, (ii) large wall potentials (relative to the plasma temperature): $\phi_W \gg 1$, and (iii) Debye length, λ_d, much smaller than thermal Larmor radius of the attracted species, λ_m. It is found that, irrespective of the angle of incidence: (i) The potential threshold for a magnetized sheath is $\phi_W = O(\lambda_d^4/\lambda_m^4)$; (ii) the characteristic magnetic length in the sheath is λ_m^3/λ_d^2, much larger than λ_m and proportional to $|\mathbf{B}|^{-3}$ and the plasma flow into the sheath; (iii) the electric field **E** increases towards the wall and produces a noncycloidal plasma drift that breaks down magnetic insulation. Plasma dynamics in a magnetized sheath consists of an **E**-aligned region, a drift region, and a **B**-aligned region. The drift region is relevant only for angles far from normal incidence and the density profile presents spatial oscillations there; for grazing incidence, the **B**-aligned region is not found. Different scaling laws of the sheath thickness versus wall potential and incidence angle are obtained; in particular, the thickness of a magnetized sheath at parallel incidence is the local Larmor radius at the wall. The applicability of the model to experiments in the ionosphere is commented. © *1999 American Institute of Physics.* [S1070-664X(99)01911-4]

I. INTRODUCTION

In a recent paper[1] we analyzed the one-dimensional (1D) structure of a weakly-collisional plasma close to a charged, planar surface, in the presence of an uniform magnetic-field **B** oblique to the wall, Fig. 1(a), using a macroscopic model of the plasma. Three length scales (associated to the attracted species) were considered in the problem: The thermal Larmor radius, λ_m, (which is inversely proportional to the strength of the magnetic field, B), the Debye length, λ_d, and a collision mean free path, λ_c, with $\lambda_d \ll \lambda_c$ for weak collisionality. Different plasma structures were found for the three distinguished limits of the two dimensionless ratios

$$\Lambda_{dm} = \lambda_d/\lambda_m, \quad \Lambda_{cm} = \lambda_c/\lambda_m.$$

In particular, for the doubly distinguished limit $\lambda_d \ll \lambda_m \ll \lambda_c$, first considered by Chodura,[2] the 1D plasma structure consists of three asymptotic regions, each one related to a different scale length, Fig. 1(c): First there is the collisional presheath, then the collisionless Chodura layer, and finally the space-charge sheath. Their typical thicknesses are λ_c, $\lambda_m \sin\psi$, and $L_{sh} = \lambda_d \phi_W^{3/4}$ (Child–Langmuir law), respectively, where ψ is the angle of incidence into the wall and ϕ_W is the potential jump across the sheath, nondimensionalized with the plasma temperature. The macroscopic velocity field of the plasma is **B**-aligned in the presheath, three-dimensional in the Chodura layer (due to the $\mathbf{E}\times\mathbf{B}$ and polarization drifts), and it becomes **E**-aligned (i.e., unmagnetized) in the space-charge sheath. Transitions between two asymptotic regions [at points C and S in Fig. 1(c)] are related to particular sonic conditions on the plasma flow.[1–3]

Since the spatial profiles of the solution are universal for any wall potential, only the sheath structure changes when ϕ_W is incremented. As the sheath thickness is proportional to $\phi_W^{3/4}$, the sheath is unmagnetized as long as ϕ_W is not too large. Some authors[4,5] infer that magnetic effects appear in the sheath when L_{sh} becomes of the order of λ_m. Using Child–Langmuir law for L_{sh}, that hypothesis yields that a sheath is magnetized when

$$\phi_W \gg O(\Lambda_{dm}^{-4/3}). \tag{1}$$

However, at the sheath entrance the electric field and the kinetic energy of the plasma change in the scale λ_d, so, for $\Lambda_{dm} \ll 1$, the characteristic length for magnetic effects can be larger than λ_m and the above estimate may not hold. It is also essential to determine, once the sheath is magnetized, whether the electric field breaks down magnetic insulation: Classical cycloidal drift motion and consequent magnetic insulation are associated to uniform electric fields, but space-charge fields produced by a single-species are not uniform.

The goal of this paper is to establish an analytical model of a magnetized sheath valid for $\Lambda_{dm} \ll 1$, $\phi_W \gg 1$, and any ψ. Compared with a particle code approach, this analytical solution will determine clearly the influence of the different dimensionless parameters and, in particular, the threshold of ϕ_W for magnetic effects—which, in fact, will not coincide with Eq. (1). Also, it will determine the spatial structure of both electric field and plasma, and will match correctly with the Chodura layer. There are few previous works dedicated to the parametric range of interest here. Auer[6] obtained the solution for the particular case $\psi = 90°$ and $\Lambda_{dm} \to 0$, which

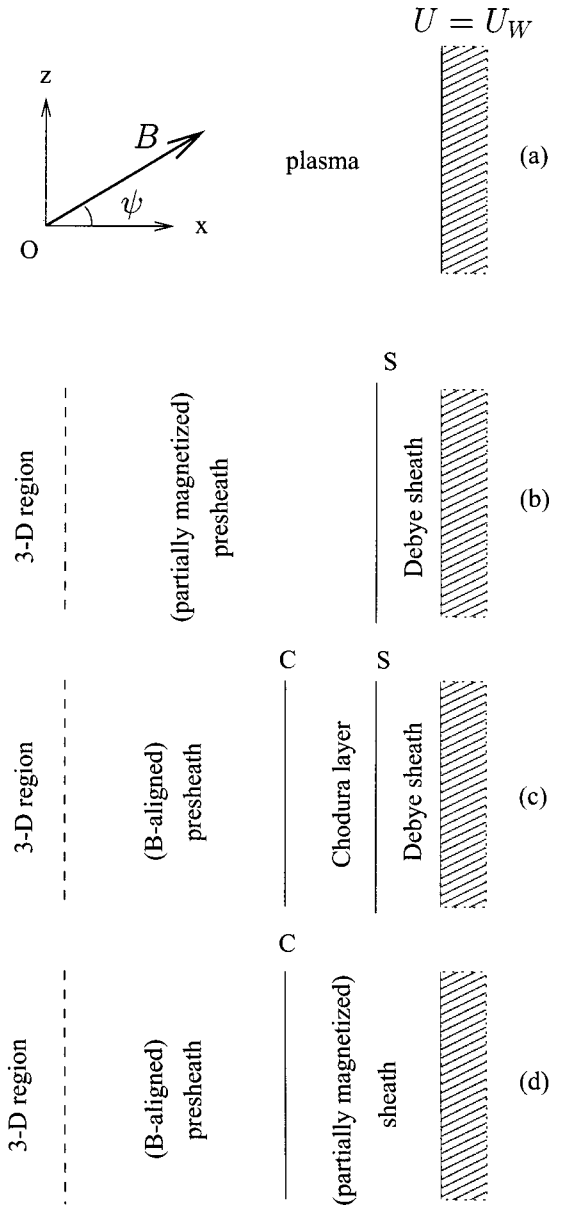

FIG. 1. (a) Sketch of the 1D model and reference frame. Plasma regions for (b) weak B:$\lambda_d \ll \lambda_m \sim \lambda_c$, (c) intermediate B:$\lambda_d \ll \lambda_m \ll \lambda_c$, and (d) strong B:$\lambda_d \sim \lambda_m \ll \lambda_c$. Transition points C and S are singular points of the plasma equations. This paper is focussed in the internal structure of the sheath for the intermediate-B case (see Fig. 4).

presents singularities for the plasma density (it will be seen here that thermal effects remove these singularities). Bergmann[7] ran numerical simulations of a supposedly magnetized sheath with $\Lambda_{dm} \sim 0.03-0.06$, $\phi_W \sim 30$, and several angles of incidence (however, we will show that for these conditions magnetic effects are limited to the entrance conditions to the sheath). Other analyses of magnetized sheaths consider parametric domains different from ours, like the kinetic model of Daybelge and Bein[8] or the numerical simulations of DeWald *et al.*[9], who discussed the range $\Lambda_{dm} \geqslant O(1)$, $|\phi_W| \leqslant O(1)$, and grazing incidence. Finally, models where the electric field is fixed instead of being determined self-consistently through Poisson equation, are omitted due to their limited interest.

The problem discussed in the paper is typically found in the ionosphere, like in spacecraft experiments on charge control[10] or on current collection. Examples of this second application are recent Tethered Satellite System (TSS)-1 and -1R missions.[11,12] TSS-1R was biased to dimensionless potentials up to 10^4 in the F-layer of the ionosphere, where Λ_{dm} is about 0.1 and 0.3, at day and night, respectively. In a different field of research, magnetized sheaths (at angles close to grazing incidence) are of interest in magnetic confinement devices.[7–9]

Planar models can analyze the local structure of the plasma near the wall but they cannot determine the plasma flow entering the 1D region, which must be obtained from the analysis of the more external, three-dimensional (3D) region around the object. This is the rather difficult, yet unsolved, problem of current collection in a magnetized plasma. The diverse theories on that problem, recently reviewed by Laframboise and Sonmor,[13] give a minor role to the space-charge sheath. In general, they either ignore totally the space-charge field or they consider the sheath as thin and unmagnetized. Furthermore, the experimental results of TSS-1 and TSS-1R do not agree with the basic, and extensively invoked, Parker–Murphy theory[14] for magnetized, collisionless plasmas. The collected currents were larger, by a factor of up to 3, than the current upper-bound established by Parker and Murphy. Diverse effects have been discussed to adapt the theory to satellite ambient conditions. However, Vannaroni *et al.*[12] have shown that the experimental current-voltage response fits better with Langmuir–Blodgett theory[15] for unmagnetized plasmas. Also, measurements with Langmuir probes in the close vicinity of TSS-1R satellite detected no magnetization of electrons, despite of satellite potential being well beyond the threshold of Eq. (1). All this suggests a revision and further investigation of magnetic theories, and this paper tries to contribute to it.

The paper is organized as follows. Section II presents the 1D model of a collisionless magnetoplasma for $\Lambda_{dm} \leqslant O(1)$ and the multiple-scale analysis used to study the asymptotic case $\Lambda_{dm} \ll 1$ and $\phi_W \gg 1$. Section III discusses, for the limit $\Lambda_{dm} = 0$, the influence of wall potential and angle of incidence on plasma dynamics and sheath structure. Final considerations are presented in Sec. IV. The singularities of the model for grazing incidence are discussed in the Appendix.

II. MODEL OF THE COLLISIONLESS REGION

A semi-infinite, magnetized plasma is bounded by a planar wall, biased to a potential U_W large enough, compared to the plasma temperature, to create a space-charge sheath around the wall. The magnetic field $\mathbf{B}$ is uniform and forms an angle ψ with the space-charge electric field, $\mathbf{E} = E\mathbf{1}_x$, Fig. 1(a). Defining unit vectors

$$\mathbf{1}_b = \mathbf{1}_x \cos\psi + 1_z \sin\psi, \quad \mathbf{1}_p = -\mathbf{1}_x \sin\psi + \mathbf{1}_z \cos\psi,$$

one has

$$\mathbf{B} = B\mathbf{1}_b, \quad \mathbf{E} = E\mathbf{1}_x = E_b\mathbf{1}_b + E_p\mathbf{1}_p, \tag{2}$$

with E_b and E_p parallel and perpendicular to **B**, respectively; the $\mathbf{E}\times\mathbf{B}$ drift is along $\mathbf{1}_y$. The plasma consists of two species, one is attracted by the wall potential (and collected by the wall) and the other one is repelled. As in Ref. 1, a two-fluid macroscopic model is used for the plasma. Let q, m, N, T, and $\mathbf{V}=(V_x,V_y,V_z)$, be the electric charge, particle mass, density, temperature, and velocity of the attracted species, respectively, and $-q$, N_r and T_r, the charge, density and temperature of the repelled species. The temperatures of both species are assumed constant (although this is not relevant for the sheath) and a Maxwell–Boltzmann distribution is assumed for the repelled species. If there is no creation of particles, the continuity equation for the attracted species reads

$$NV_x=\text{const}=\Gamma_x, \tag{3}$$

where the plasma flow Γ_x entering into the 1D region is a parameter of the model. Notice, first, that the validity of this one-stream model is restricted to solutions that do not cross $V_x=0$, in which case a multistream or a kinetic model should be used. Second, one can write

$$\Gamma_x(\psi)=g(\psi)\Gamma_{\text{th}}, \tag{4}$$

where Γ_{th} is the thermal flow of the undisturbed plasma and $g(\psi)$ is the relative flow, which can be ψ-dependent. The determination of $g(\psi)$ is beyond the possibilities of a planar model, and any consistent prediction of it must be based on the solution of the 3D collection problem (that would include the actual object geometry). A common assumption[7,14] is $g(\psi)\propto\cos\psi$, which means to neglect totally the flow transversal to **B**. This assumption seems too extreme in practice and, indeed, leads to no solution for grazing incidence.

Characteristic magnitudes to nondimensionalize the plasma equations are a density

$$N_*=\Gamma_x(m/T)^{1/2},$$

(T is in energy units), the Debye length

$$\lambda_d=(\epsilon_0 T/q^2N_*)^{1/2}, \tag{5}$$

(ϵ_0 is the vacuum permittivity), and the thermal Larmor radius

$$\lambda_m=(Tm)^{1/2}/qB, \tag{6}$$

B and ψ can be defined such that $qB>0$, and it suffices to consider angles between 0° and 90°. The Debye-to-magnetic length ratio (also the gyro-to-plasma frequency ratio) is

$$\Lambda_{dm}=|B|\sqrt{\epsilon_0/mN_*}, \tag{7}$$

which is independent of T. Notice that the Debye length defined in Eq. (5) is based on the flow into the planar region; from Eq. (4), it is proportional to $g^{-1/2}$ times the Debye length of the undisturbed plasma, $\lambda_{d\infty}$.

The first set of dimensionless variables to be used is

$$\xi=\frac{x}{\lambda_d},\quad n=\frac{N}{N_*},\quad n_r=\frac{N_r}{N_*},\quad \phi=-\frac{qU}{T},$$

$$\mathbf{v}=\frac{\mathbf{V}}{\sqrt{T/m}},\quad t_r=\frac{T_r}{T};$$

notice that for a monotonic potential it is $\phi>0$, independently of the sign of U_W. For λ_d and λ_m much smaller than the collision mean-free path λ_c, the dimensionless equations pertinent to a collisionless plasma are[1]

$$\left(v_x-\frac{1}{v_x}\right)\frac{dv_x}{d\xi}=\frac{d\phi}{d\xi}+\Lambda_{dm}v_y\sin\psi, \tag{8}$$

$$v_x\frac{dv_y}{d\xi}=\Lambda_{dm}(v_z\cos\psi-v_x\sin\psi), \tag{9}$$

$$v_x\frac{dv_z}{d\xi}=-\Lambda_{dm}v_y\cos\psi, \tag{10}$$

$$\frac{d^2\phi}{d\xi^2}=\frac{1}{v_x}-n_r, \tag{11}$$

$$n_r=n_{rC}\exp\frac{-\phi}{t_r}. \tag{12}$$

The electric and velocity fields are coupled through the density of the attracted species $n=1/v_x$. The transition point C from the collisional presheath to the collisionless region is defined by condition $\lambda_c d\phi/dx=\infty$ in the presheath equations (not written here); then these equations yield that the plasma enters sonically and B-aligned into the collisionless region.[1] In variable ξ, and for $\psi\neq 90°$ and $\Lambda_{dm}\leqslant O(1)$, boundary conditions at the collisionless side of point C are

$$\begin{aligned}&\xi_C=-\infty,\quad \mathbf{v}_C=c_s(\cos\psi,0,\sin\psi),\\ &n_{rC}=\frac{1}{v_{xC}},\quad \left.\frac{1}{\Lambda_{dm}}\frac{d\phi}{d\xi}\right|_c=0,\end{aligned} \tag{13}$$

with $c_s=\sqrt{1+t_r}$ the dimensionless sound speed of the plasma, and we set $\phi_C=0$. Equations (8)–(12) admit two first integrals[1] related to the conservation of energy and momentum along **B**,

$$\begin{aligned}&(v_x^2+v_y^2+v_z^2)/2-\ln v_x-\phi=c_s^2/2-\ln c_s,\\ &v_x\cos\psi+v_z\sin\psi+\left[\frac{1}{v_x}+t_rn_r-\frac{1}{2}\left(\frac{d\phi}{d\xi}\right)^2\right]\cos\psi=2c_s.\end{aligned} \tag{14}$$

These conservation laws reduce by two the order of Eqs. (8)–(11).

Equations (8)–(13) have a unique and regular solution for any ϕ_W, Λ_{dm}, and ψ (with $\psi\neq 90°$). For $\Lambda_{dm}\geqslant O(1)$ the solution consists of a practically B-aligned sheath (with a marginal $\mathbf{E}\times\mathbf{B}$ drift) and there is no Chodura layer, Fig. 1(d). For $\Lambda_{dm}\ll 1$, the solution is more complex and asymptotic techniques are used to reveal it. First, a two-scale analysis shows that the collisionless region is divided into the quasineutral Chodura layer and the space-charge sheath. The solution for the Chodura layer is obtained by modifying Eqs. (8)–(11), using

$$\zeta=x/\lambda_m=\Lambda_{dm}\xi,$$

as spatial variable, instead of ξ, and taking then the quasineutral limit $\Lambda_{dm}\to 0$; in particular, Eq. (11) becomes $n\simeq n_r$. The Chodura layer extends from point C to point S where

$$v_{xS}=c_s,\quad d\phi/d\zeta|_S=\pm\infty,\quad \phi_S=\phi_C-\ln\cos\psi,$$

and v_{yS} and v_{zS} are obtained from Eq. (14). Point S marks the entrance to the non-neutral sheath, where ξ is the natural spatial variable. In this variable, point S is at $\xi_S=-\infty$ and the electric field is

$$d\phi/d\xi|_S=\Lambda_{dm}d\phi/d\zeta|_S\simeq 0.$$

Since point S is singular for the sheath equations, the asymptotic solution at $-\xi\gg 1$ is needed as ''initial'' condition for a regular integration of Eqs. (8)–(11).

The equations of a magnetized sheath admit simplifications for $\phi\gg 1$ that lead to a new analytical solution. Since

$$n_r\sim n_{rC}\exp(-\phi/t_r),\quad v_x\sim\phi^{1/2}, \tag{15}$$

$1/v_x$ and n_r can be dropped from the left-hand side of Eq. (8) and the right-hand side of Eq. (11), respectively, when $\phi\gg 1$ (for any Λ_{dm}). This means to neglect thermal effects, so the resultant equations correspond to a cold-plasma (or hypersonic) magnetized sheath. The general solution of these cold-plasma equations (valid for $\phi\gg 1$) is

$$\begin{aligned}
\tilde{v}_x&=1/\tilde{n}=(\tau^2/2)\cos^2\psi+1-c_1\cos\psi\\
&\quad+(c_3\sin\tau-c_2\cos\tau)\sin\psi,\\
\tilde{v}_y&=-\tau\sin\psi+c_3\cos\tau+c_2\sin\tau,\\
\tilde{v}_z&=(\tau^2/2)\cos\psi\sin\psi-c_1\sin\psi\\
&\quad-(c_3\sin\tau-c_2\cos\tau)\cos\psi,\\
\tilde{\phi}&=\int\tilde{v}_x\tau dt+c_4=\tfrac{1}{2}(\tilde{v}_x^2+\tilde{v}_y^2+\tilde{v}_z^2)+\text{const},\\
\tilde{x}&=\int\tilde{v}_x d\tau+c_5,
\end{aligned} \tag{16}$$

where

$$\tilde{x}=\Lambda_{dm}^3\xi,\quad \tilde{\mathbf{v}}=\Lambda_{dm}^2\mathbf{v},\quad \tilde{\phi}=\Lambda_{dm}^4\phi,\quad \tilde{n}=\Lambda_{dm}^{-2}n, \tag{17}$$

are the convenient dimensionless variables for the cold-plasma model; the independent parameter τ is *both* the electric field

$$d\tilde{\phi}/d\tilde{x}=\tau, \tag{18}$$

and the transit time in the sheath of a plasma element (an average over individual particles in this macroscopic theory); and constants c_1 to c_5 are obtained matching, at $\tilde{\phi}\gg\Lambda_{dm}^4$, solution (16) and the numerical solution of the exact equations.

Figure 2 shows plasma profiles in the whole collisionless region for different Λ_{dm}; dashed lines correspond to the continuation of the exact solution with hypersonic solution (16). For $\Lambda_{dm}\ll 1$ the regions to the left and to the right of $\tilde{v}_x\simeq c_s\Lambda_{dm}^2$ (point S) correspond to the Chodura layer and the space-charge sheath, respectively. The cases $\Lambda_{dm}\ll 1$ and $\Lambda_{dm}\geqslant O(1)$ differ in the region $\tilde{x}\leqslant O(1)$, close to the entrance, where the motion is E-aligned for $\Lambda_{dm}\ll 1$, and B-aligned for $\Lambda_{dm}\gg 1$. When $\tilde{x}\gg 1$, the motion is B-aligned for any Λ_{dm}. Notice that $\tilde{v}_y(\tilde{x})$, caused by the $\mathbf{E}\times\mathbf{B}$ drift, is quite insensitive to Λ_{dm} (from point C on).

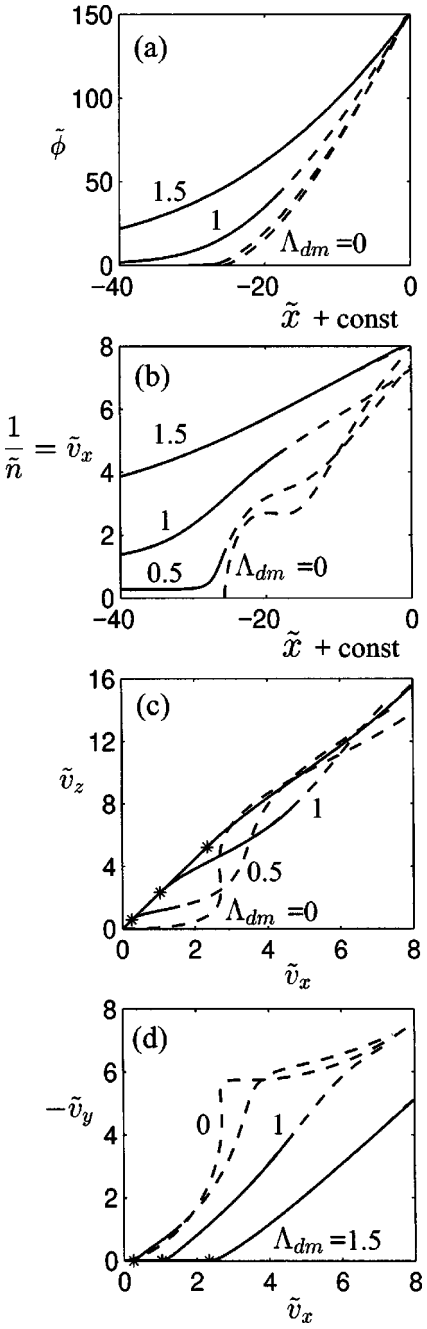

FIG. 2. Plasma response for $\psi=66°$, $t_r=5.5$, and $\Lambda_{dm}=0$, 0.5, 1, and 1.5; $\tilde{\phi}_C=0$. Solid and dashed lines correspond to exact and hypersonic solutions, respectively; they have been matched at $\phi=\tilde{\phi}\Lambda_{dm}^{-4}\sim 20$ where $\tilde{v}_x^2$, $\tilde{v}_x\tilde{n}_r<0.1$. In (c) and (d): The asterisk represents point C and the region to the left of this point is the B-aligned, collisional presheath.

III. THE COLD-PLASMA, MAGNETIZED SHEATH

From definition (17) one may write $\tilde{x}=x/\lambda_m^s$ with

$$\lambda_m^s=\frac{\lambda_m^3}{\lambda_d^2}=\frac{m^2\Gamma_x}{qB^3}, \tag{19}$$

so λ_m^s is presumably the characteristic length of a cold-plasma, magnetized sheath. Also, in the new variables (17), the nonhypersonic region, $\phi=O(1)$, corresponds to

$$\tau\leqslant O(\Lambda_{dm}),\quad \tilde{x}\leqslant O(\lambda_{dm}^3),\quad \tilde{\phi}\leqslant O(\Lambda_{dm}^4), \tag{20}$$

$$\tilde{v} \leqslant O(\Lambda_{dm}^2).$$

These features make the hypersonic solution (16) especially simple and interesting in the asymptotic limit $\Lambda_{dm} \to 0$. First, scale λ_m^s of the cold-plasma sheath is much larger than λ_d and λ_m, so both the Chodura layer and the nonhypersonic sheath subregion, are reduced to the entrance point

$$\tau \to 0, \quad \tilde{\phi} \to 0, \quad \tilde{\mathbf{v}} \to 0, \tag{21}$$

of the cold-plasma solution. Next, these conditions determine c_1 to c_5 analytically,

$$c_1 = \cos\psi, \quad c_2 = \sin\psi, \quad c_3 = c_4 = c_5 = 0,$$

and solution (16) simplifies to

$$\begin{aligned}
\tilde{v}_x &= 1/\tilde{n} = (\tau^2/2)\cos^2\psi + (1-\cos\tau)\sin^2\psi, \\
\tilde{v}_y &= (\sin\tau - \tau)\sin\psi, \\
\tilde{v}_z &= (\tau^2/2 - 1 + \cos\tau)\cos\psi\sin\psi, \\
\tilde{\phi} &= (\tau^4/8)\cos^2\psi + (\tau^2/2 + 1 - \cos\tau - \tau\sin\tau)\sin^2\psi, \\
\tilde{x} &= (\tau^3/6)\cos^2\psi + (\tau - \sin\tau)\sin^2\psi.
\end{aligned} \tag{22}$$

This solution is regular for any $\tau > 0$ and $\psi \neq 90°$. For $\psi = 0$, it recovers the well-known solution of a cold-plasma, unmagnetized sheath. For $\phi_W \gg 1$ and $\Lambda_{dm} \ll 1$, solution (22) covers practically all the collisionless region, which is finite in variable $\tilde{x}$.

Figure 2 depicted solution (22) for $\psi = 66°$; one sees that the cold-plasma solution is a good approximation for $\Lambda_{dm} < 0.5$. Figure 3 shows solution (22) for different incidence angles. A first salient feature is that $\tilde{v}_x$ and $\tilde{n}$ present nonmonotonic profiles for large incidence angles. For ψ given, the position and number of the local extrema of $\tilde{n}(\tilde{x})$ correspond to $d\tilde{v}_x/d\tau = 0$, that is to the solutions of

$$-\tau^{-1}\sin\tau = \cot^2\psi.$$

The analysis of this equation yields that oscillations appear for $\psi > 66°$, approximately (see Fig. 2), and $\pi/2 < \tau < 1/\cos^2\psi$, and their number and amplitude increase with ψ. For $\cos\psi \ll 1$, the first minimum and maximum are $\tilde{n} \sim 1/(2\sin^2\psi) \sim \frac{1}{2}$ and $\tilde{n} \sim 1/(2\pi^2\cos^2\psi)$, and they are reached at $\tilde{\phi} \sim \pi^2/2 \simeq 4.9$ and $\tilde{\phi} \sim 2\pi^2 \simeq 19.7$, respectively. The ratio between these extrema is $\tan^2\psi/\pi^2$, so oscillations larger than 100%, relative to the mean value, are observed for $\psi \geqslant 77.3°$.

For $\psi = 90°$, it is $\tilde{v}_x = 0$ at τ a multiple of 2π yielding $\tilde{n} = \infty$. A detailed analysis of this local problem is presented in the Appendix. The inclusion of thermal effects removes the singularity and the local maxima of density are of the order of the external one: $n = \tilde{n}\Lambda_{dm}^2 \leqslant O(1)$. The cold-plasma solution is thus asymptotically valid for any wall potential and incidence angle.

In spite of spatial oscillations, it is $\tilde{n} > 0$, so Poisson equation yields that the electric field increases monotonically from the sheath entrance to the wall for all angles of incidence, Fig. 3(a). At the same time, the nonuniformity of the electric field characterizes the competition between electric and magnetic effects on the plasma motion. The velocity

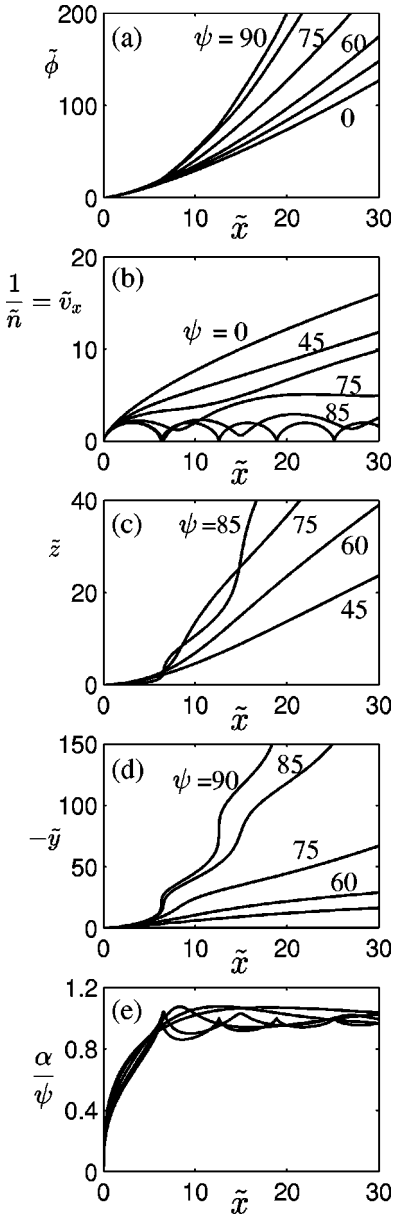

FIG. 3. Cold plasma sheath profiles for ψ(in degrees) = 0, 45, 60, 75, 85, and 90. (a) Potential, (b) inverse of density, (c)–(d) plasma trajectory, $\tilde{\mathbf{r}} = \mathbf{r}/\lambda_m^s$, and (e) angle of penetration. Part (a) also represents $\tilde{\phi}_W(\tilde{L}_{sh})$.

field is the linear combination of the response to the components E_b and E_p of **E**, Eq. (2): the component $\tau\cos\psi$, parallel to **B**, yields a parallel velocity

$$\tilde{v}_b = (\tau^2/2)\cos\psi \mathbf{1}_b,$$

and the component $\tau\sin\psi$, orthogonal to **B**, produces a drift velocity

$$\tilde{\mathbf{v}}_{dr} = \sin\psi[(\sin\tau - \tau)\mathbf{1}_y - (1-\cos\tau)\mathbf{1}_p].$$

Integration of this cycloidal drift velocity yields a *noncycloidal* drift trajectory

$$\int \tilde{\mathbf{v}}_{dr} d\tau = \sin\psi[(1 - \cos\tau - \tau^2/2)\mathbf{1}_y - (\tau - \sin\tau)\mathbf{1}_p];$$

the plasma trajectory is shown in Figs. 3(c) and 3(d). Therefore, whereas the drift motion is cycloidal (and thus bounded

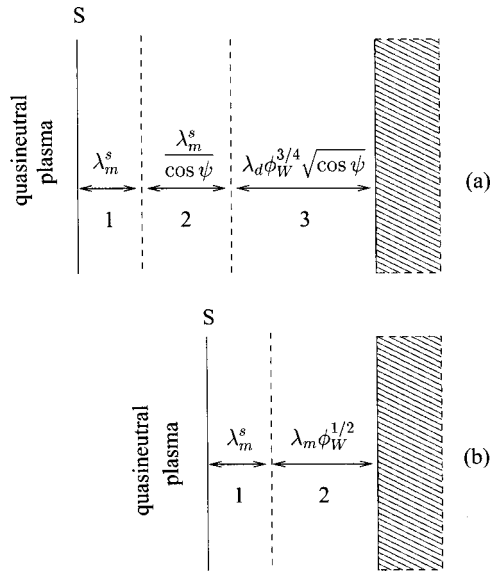

FIG. 4. Structure of the space-charge sheath and typical thickness of each asymptotic subregion for $\Lambda_{dm} \ll 1$, (a) $\psi \neq 90°$ and $\phi_W \gg \Lambda_{dm}^{-4} \tan^2\psi$, (b) $\psi = 90°$ and $\phi_W \gg \Lambda_{dm}^{-4}$. Region 1 is *E*-aligned (unmagnetized), region 2 is dominated by the $\mathbf{E}\times\mathbf{B}$ drift, and region 3 is *B*-aligned. Thermal effects affect a small layer of thickness λ_d close to point *S* only. There are not well-defined transitions among the sheath subregions. As ϕ_W decreases the region most to the right decreases and eventually disappears.

along $\mathbf{1}_p$) for a uniform electric field, the monotonic electric field of the sheath breaks down the magnetic insulation of the incoming plasma. This is essential for grazing incidence, where only the perpendicular drift can bring the particles to the wall.

The competition between the components of $\mathbf{E}$ parallel and perpendicular to $\mathbf{B}$ leads to different *asymptotic* subregions within the sheath. For large incidence angles ($\cos\psi \ll 1$) there are up to three subregions:

(i) An *E-aligned* region for $\tilde{x} \ll 1$, where magnetic effects are marginal and the plasma motion is basically along Ox with

$$\tau \simeq (6\tilde{x})^{1/3}, \quad \tilde{\phi} \simeq (81\tilde{x}^4/32)^{1/3}, \quad \tilde{v}_x = 1/\tilde{n} \simeq (9\tilde{x}^2/2)^{1/3},$$
$$\tilde{v}_y \simeq -\tilde{x}\sin\psi, \quad \tilde{v}_z \simeq (3\tilde{x}^4/32)^{1/3}\cos\psi\sin\psi. \tag{23}$$

(ii) A *drift* region for $1 \ll \tilde{x} \ll 1/\cos\psi$, dominated by the $\mathbf{E}\times\mathbf{B}$ drift, where the potential and velocity fields verify

$$\tau \simeq \tilde{x}, \quad \tilde{\phi} \simeq \tilde{x}^2/2, \quad \hat{v}_x = 1/\tilde{n} \simeq 1 - \cos\tilde{x} + O(\tilde{x}\cos\psi),$$
$$\tilde{v}_y \simeq -\tilde{x} \quad \tilde{v}_z \simeq (1/2)\tilde{x}^2\cos\psi. \tag{24}$$

(iii) A *B-aligned* region for $\tilde{x} \gg 1/\cos\psi$, where the $\mathbf{E}\times\mathbf{B}$ drift is marginal again and the plasma moves along $\mathbf{1}_b$ with

$$\tau \simeq (6\tilde{x}/\cos^2\psi)^{1/3}, \quad \tilde{\phi} \simeq (81\tilde{x}^4/32\cos^2\psi)^{1/3},$$
$$\tilde{v}_x = 1/\tilde{n} \simeq (9\tilde{x}^2\cos^2\psi/2)^{1/3},$$
$$\tilde{v}_y \simeq -(6\tilde{x}/\cos^2\psi)^{1/3}\sin\psi, \tag{25}$$
$$\tilde{v}_z \simeq (9\tilde{x}^2\cos^2\psi/2)^{1/3}\tan\psi.$$

The three subregions and their typical thicknesses are sketched in Fig. 4(a). For small or moderate angles of incidence: $\cos\psi = O(1)$, the asymptotic drift region disappears, and for grazing incidence: $\cos\psi = 0$, there is not a *B*-aligned region, Fig. 4(b). Spatial oscillations of the plasma density are due to the drift motion and thus take place only in the drift region. The electric field τ is proportional to $\tilde{x}^{1/3}$ in the *E*-aligned and *B*-aligned regions but it is practically linear with $\tilde{x}$ in the drift region (as if $\tilde{n} \simeq 1$ on the average). The angle of penetration of a particle through the sheath,

$$\alpha = \arccos\frac{\tilde{v}_x}{|\tilde{\mathbf{v}}|} \simeq \arccos\frac{\tilde{v}_x}{\sqrt{2\tilde{\phi}}},$$

is depicted in Fig. 3(e); it changes from 0 to ψ, from the *E*-aligned to the *B*-aligned region. For $\phi = \phi_W$, α is the angle of impact with the wall, of interest to evaluate surface sputtering.

The asymptotic analysis of the sheath subregions concludes that, for any angle of incidence, the sheath is affected by the magnetic field when $\tilde{\phi} \geqslant O(1)$, i.e., when

$$\phi \geqslant O(\Lambda_{dm}^{-4}). \tag{26}$$

At the potential threshold for magnetic effects, the sheath thickness turns to be $x \sim \lambda_m^s$, which confirms that $\lambda_m^s \equiv \lambda_m^3/\lambda_d^2$, is the characteristic magnetic length in the sheath. At any point, the sheath thickness coincides with the local scale of change of the potential: $(d\ln U/dx)^{-1}$, which is also the local scale of change of the plasma kinetic energy. An intuitive and correct derivation of condition (26) is obtained from equating the sheath thickness taken from the unmagnetized Child–Langmuir law, to the *local* Larmor radius of a particle

$$\lambda_d\phi^{3/4} \sim \lambda_m\phi^{1/2}.$$

Therefore the magnetic field starts to affect where the local Larmor radius becomes of the order of the local scale of change of the plasma energy.

Since the sheath solution is universal for any $\tilde{\phi}_W$, the evolution of the dimensionless sheath thickness, $\tilde{L}_{sh} = L_{sh}/\lambda_m^s$, with $\tilde{\phi}_W$ is given by function $\tilde{\phi}(\tilde{x})$, Fig. 3(a). Asymptotic scaling laws for $L_{sh}(\phi_W, \psi)$ are obtained from Eqs. (23)–(25)

$$L_{sh} \simeq \begin{cases} \lambda_d(2^{5/4}/3)\phi_W^{3/4}, & \text{for } \phi_W \ll \Lambda_{dm}^{-4}, \\ \lambda_m 2^{1/2}\phi_W^{1/2}, & \text{for } \Lambda_{dm}^{-4} \ll \phi_W \ll \Lambda_{dm}^{-4}\cos^{-2}\psi, \\ \lambda_d(2^{5/4}/3)\phi_W^{3/4}\cos^{1/2}\psi, & \text{for } \phi_W \gg \Lambda_{dm}^{-4}\cos^{-2}\psi. \end{cases} \tag{27}$$

The second and third expressions correspond to magnetized sheaths. The third one is still a Child–Langmuir law with factor $\cos^{1/2}\psi$ coming from the fact that the plasma moves along $\mathbf{B}$ while spatial gradients are along $\mathbf{E}$. The second expression makes sense only for large angles of incidence and, in particular, for a magnetized sheath at grazing incidence; it says that L_{sh} is equal to the local Larmor radius of a particle at the wall. The dependence on λ_m, instead of on λ_d as Poisson equation suggests, is due to the plasma density n being of order λ_d^2/λ_m^2.

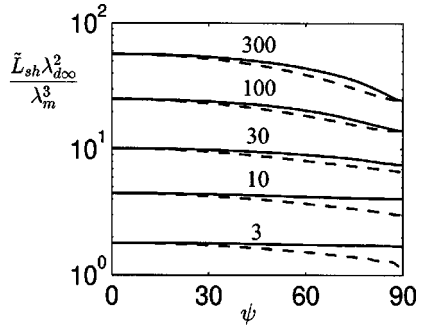

FIG. 5. Variation of the sheath thickness with the angle of incidence for $\phi_W\lambda_{d\infty}^4/\lambda_m^4=3$, 10, 30, 100, and 300, and $\lambda_{d\infty}=\lambda_d g^{-1/2}(\psi)$ with $g(\psi)=1$ in solid lines and $g(\psi)=(1+\cos\psi)/2$ in dashed lines.

For plasma flow Γ_x independent of ψ [i.e., $g(\psi)=1$ in Eq. (4)] Eq. (27) and Fig. 3(a) show that larger angles of incidence imply larger plasma densities, larger electric fields, and, therefore, thinner sheaths. Figure 5 shows the variation of the sheath thickness with the angle of incidence for two different expressions of $g(\psi)$; these plots also represent the sheath shape around a thick cylinder of axis perpendicular to **B**. Observe first that, although $g(\psi)$ is essential to compute the current collected at the wall, it has a small influence on the shape of a magnetized sheath, as the solid and dashed lines for $\tilde{\phi}_W>30$ show. Second, the case $\tilde{\phi}_W\sim 3$ corresponds to a weakly magnetized sheath (as the solid line indicates) and the variation of thickness shown by the dashed line comes from the dependence on ψ of the flow entering the sheath (due to magnetic effects *outside* the sheath). The results presented by Bergmann[7] on magnetic effects in a sheath correspond to this second case and not to a magnetized sheath. His numerical simulations use entrance condition (13) and $g(\psi)\propto\cos\psi$. Applying threshold condition (26) to his simulation parameters one finds that the sheaths he obtained are unmagnetized, with the dependence on ψ being due to entrance conditions exclusively. Indeed the only scaling law he found for the sheath thickness was $L_{sh}\propto\lambda_{d\infty}\phi_W^{3/4}\cos^{-1/2}\psi$, which agrees with the first expression of Eq. (27) when $\lambda_{d\infty}\propto\lambda_d g^{-1/2}(\psi)$.

IV. FINAL CONSIDERATIONS

We have presented a model of the space-charge sheath which completes a planar model of the plasma structure around a biased wall, oblique to a uniform magnetic field, for $\lambda_d\ll\lambda_m\ll\lambda_c$ and large wall potentials. Except in a thin layer of thickness λ_d, thermal effects can be removed from the sheath equations, which then have an analytical solution. Plasma dynamics are the consequence of the spatial profile of the electric field. This is monotonic for any angle of incidence (including $\psi=90°$) and leads to $|\mathbf{v}(x)|$ monotonic and an unbounded plasma drift, which breaks down magnetic insulation. This allows the plasma to be collected at grazing incidence for any value of the wall potential (a uniform electric field, whatever strong, would lead to a magnetically insulated solution for ϕ_W large enough and ψ close to 90°).

The inhomogeneity of the electric field produces up to three subregions in the sheath, Fig. 4(a), with different plasma dynamics. These subregions together with the (quasineutral) collisional presheath and Chodura layer, Fig. 1(c), constitute the complete planar structure of the plasma. From the far and weakly disturbed region to the wall, the plasma trajectory changes from *B*-aligned, to *E*-aligned, and then to *B*-aligned again. These changes take place in two intermediate regions (one quasineutral and one non-neutral) dominated by the $\mathbf{E}\times\mathbf{B}$ drift. The two drift regions increase with the angle of incidence; in the drift region within the sheath (but not in the Chodura layer) the nonmonotonicity of the velocity component perpendicular to the wall leads to a nonmonotonic density profile. For $\psi=90°$, thermal effects must be kept around the density maxima to obtain a regular solution. The diversity of sheath regions are explained by the competition between the local Larmor radius and the local scale of change of plasma energy. At the sheath entrance the second scale is the shorter one and the motion is *E*-aligned. Since this scale increases faster than the gyroradius along the sheath, magnetic effects eventually appear. (A similar argument was valid to interpret the change of plasma trajectory in the Chodura layer.[1]) The final *B*-aligned region is also due to the increasing electric field, which produces a stronger acceleration of the plasma along **B** than perpendicular to it.

The model determines that the threshold of ϕ_W for a magnetized sheath is of the order of λ_m^4/λ_d^4, much larger, for $\Lambda_{dm}\ll 1$, than estimate (1) proposed previously. Indeed the characteristic magnetic length in the sheath is not the thermal Larmor radius but $\lambda_m^s=\lambda_m\Lambda_{dm}^{-2}$, Eq. (19), which is proportional to $B^{-3}\Gamma_x$, the dependence on Γ_x being due to the influence of the plasma density on the electric field profile.

As an application of the model let us consider an electron attracting ($U_W>0$) object in the low Earth ionosphere. For $\lambda_d\sim 0.25$ cm and $\lambda_m\sim 2.5$ cm as typical parameters at daylight, the characteristic magnetic length in the sheath is $\lambda_m^s\sim 2.5$ m and the potential threshold for magnetic effects is $U_W\sim 1000$ V, instead of $U_W\sim 22$ V given by Eq. (1). Then, at daylight, a sheath two meter thick (and quasiplanar) is still unmagnetized (a preliminary estimate suggests that the potential threshold can be larger for a spherical sheath). On the other hand, Eq. (26) indicates that magnetic effects in the sheath depend heavily on the plasma density: In the low ionosphere, when the density decreases by one order of magnitude from day to night, the potential threshold is reduced to $U_W\sim 10$ V.

In TSS-1 and TSS-1R experiments, a spherical satellite of radius $R=0.8$ m was biased to a range of large voltages. Most experimental observations verified that $\phi_W(\lambda_d/R)^{4/3}=O(1)$ and $\phi_W\Lambda_{dm}^4\leqslant O(1)$ (although some uncertainty on $\lambda_d/\lambda_{d\infty}$ must be admitted). The first condition means that spherical effects could not be strong in the sheath and the present theory may be applied qualitatively, at least. The second condition implies that magnetic alignment of the plasma was not strong in the sheath, in agreement with on situ measurements[12] with Langmuir probes of the electron trajectory. It further implies that the current collected by the satellite had to be the current that entered into the sheath, what could explain the good fitting of the results with the Langmuir–Blodgett scaling law (based precisely in the sheath outer boundary as effective collection area). Although

the central issue, how the complex processes in the external region determine the flow function $g(\psi)$, remains to be understood, one may already conclude that both the thick sheath and the quasineutral region are influencing the current-voltage response. In other words, the rich structure of the electric potential should not be ignored by a current collection theory. A specific analysis of the plasma behavior around TSS-1R, intended to confirm the above arguments, is in progress.

ACKNOWLEDGMENTS

This research was supported by Ministerio de Educación y Cultura of Spain (Project PB97-0574-C04-02).

APPENDIX: GRAZING INCIDENCE

This is a singular case of both the collisionless, quasineutral model, Eqs. (8)–(13), and the cold-plasma sheath model, Eqs. (22). For $\psi=90°$, it is $v_{xC}=0$ at point C, Eq. (13), and there is no solution of the collisionless, quasineutral model, because there is no mechanism to transport the plasma along O_x. Collisions must be kept in the model to create a diffusion electric field that initiates the transversal transport.[3] There is then a unique set of equations for the whole quasineutral region, which extends from $\mathbf{v}\simeq\mathbf{0}$ to point S. For $\lambda_c \gg \lambda_m \gg \lambda_d$ its characteristic extension is $\lambda_m[\ln(\lambda_c/\lambda_m)]^{-1/2}$, and, although there is not a well-defined point C, a collisional and a Chodura subregions are still distinguished.[1]

For $\psi=90°$ Eqs. (8)–(12) are valid for the sheath, boundary conditions at point S are

$$\xi_S=-\infty, \quad v_{xS}=c_s,$$

$$v_{yS}\simeq -c_s\sqrt{2\ln(\lambda_c/\lambda_m)} \quad n_{rS}=1/c_S, \quad d\phi/d\xi|_S\simeq 0,$$

and we set $\phi_S=0$. Sheath equations are integrated as for $\psi\neq 90°$ and conditions (15) are verified when $\phi\gg 1$. Therefore, the cold-plasma solution (22) is formally valid also for parallel incidence (this was the particular solution obtained by Auer[6]). However, in this solution $\tilde{n}$ becomes infinity (i.e., $\tilde{v}_x=0$) at τ a multiple of 2π. Since cold-plasma hypotheses require that $\tilde{v}_x \gg \Lambda_{dm}^2$, further analysis of the regions close to the minima of $\tilde{v}_x$ is needed to accept that solution.

An integral equation for the plasma momentum provides the necessary arguments. For $\psi=90°$, Eqs. (8)–(11) yield

$$v_x+\frac{1}{v_x}-\Lambda_{dm}^2\frac{v_x^2}{2}+\Lambda_{dm}^2\ln v_x-\frac{F^2}{2}+t_r n_r + \Lambda_{dm}\int n_r v_y d\xi=\text{const}, \tag{A1}$$

where

$$F=\frac{d\phi}{d\xi}+\Lambda_{dm}v_y,$$

and the constant on the right-hand side is obtained from conditions at point S. When $\Lambda_{dm}\ll 1$, Eq. (A1) admits approximate expressions in the nonhypersonic and hypersonic regions. When $\phi=O(1)$ one has

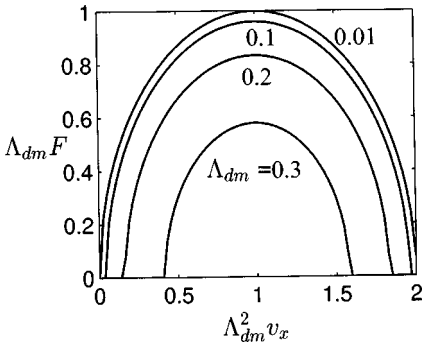

FIG. 6. Grazing incidence: Solution of Eq. (A2) for $c=2$ and different values of Λ_{dm}.

$$v_x+\frac{1}{v_x}-\frac{1}{2}\left(\frac{d\phi}{d\xi}\right)^2+t_r n_r\simeq\text{const},$$

which coincides with the conservation of momentum of an unmagnetized sheath. When $\phi\gg 1$, the presence of the repelled species is totally negligible: $n_r\sim\exp(-\phi/t_r)$, the integral term $\int_{\xi_S}^{\xi} n_r v_y d\xi$ becomes constant, and Eq. (A1) simplifies to

$$v_x+\frac{1}{v_x}-\Lambda_{dm}^2\frac{v_x^2}{2}+\Lambda_{dm}^2\ln v_x-\frac{F^2}{2}=2c, \tag{A2}$$

with constant $c-c_s$ positive and of order Λ_{dm}. Figure 6 plots Eq. (A2) for $c=2$ and several Λ_{dm}. The density $n=\Lambda_{dm}^2/\tilde{v}_x$ has extrema at $F=0$; for $\Lambda_{dm}\to 0$, these are $\Lambda_{dm}^4/2$ and $c-\sqrt{c^2-1}=O(1)$. Therefore, the maximum of n is of the order of the density at the entrance to the sheath. This confirms the asymptotic validity of the cold-plasma solution for $\psi=90°$.

Notice that, for $\Lambda_{dm}\to 0$, Eq. (A2) recovers the cold-plasma expression

$$\tilde{v}_x-\frac{\tilde{v}_x^2}{2}-\frac{\tilde{F}^2}{2}=0,$$

with $\tilde{F}\equiv\Lambda_{dm}F=\tau+\tilde{v}_y$; this equation is also obtained from solution (22). Finally, as Λ_{dm} increases the sheath tends to be B-aligned at smaller potentials and the amplitude and number of the oscillations decrease, as can be deduced from the curves of Fig. 6.

[1] E. Ahedo, Phys. Plasmas **4**, 4419 (1997).
[2] R. Chodura, Phys. Fluids **25**, 1628 (1982).
[3] K. Riemann, Phys. Plasmas **1**, 552 (1994).
[4] J. G. Laframboise and J. Rubinstein, Phys. Fluids **19**, 1900 (1976).
[5] E. Szuszczewicz and P. Takacs, Phys. Fluids **22**, 2424 (1979).
[6] P. L. Auer, Phys. Fluids **24**, 1212 (1981).
[7] A. Bergmann, Phys. Plasmas **1**, 3598 (1994).
[8] U. Daybelge and B. Bein, Phys. Fluids **24**, 1190 (1981).
[9] A. DeWald, A. Bailey, and J. Brooks, Phys. Fluids **30**, 267 (1987).
[10] N. Myers, W. J. Raitt, A. White, P. M. Banks, B. E. Gilchrist, and S. Sasaki, J. Spacecr. Rockets **27**, 25 (1990).
[11] M. Dobrowolny, U. Guidoni, E. Melchioni, G. Vannaroni, and J. P. Lebreton, J. Geophys. Res. **100**, 953 (1995).
[12] G. Vannaroni, M. Dobrowolny, J. Lebreton, E. Melchioni, F. de Venuto, C. Harvey, L. Iess, U. Guidoni, C. Bonifazi, and F. Mariani, Geophys. Res. Lett. **25**, 749 (1998).
[13] J. G. Laframboise and L. J. Sonmor, J. Geophys. Res. **98**, 337 (1993).
[14] L. Parker and B. Murphy, J. Geophys. Res. **72**, 1631 (1967).
[15] I. Langmuir and K. Blodgett, Phys. Rev. **23**, 49 (1924).